Structural Damage Analysis of Masonry Walls using Computational Homogenization

T.J. Massart, R.H.J. Peerlings, M.G.D. Geers

Structural Damage Analysis of Masonry Walls using Computational Homogenization

T. J. MASSART*
Structural and Material Computational Mechanics Dept. CP 194/5
Université Libre de Bruxelles, Av. F.-D. Roosevelt 50
1050 Brussels, Belgium

R. H. J. PEERLINGS AND M. G. D. GEERS
Department of Mechanical Engineering
Eindhoven University of Technology
P.O. Box 513, 5600 MB Eindhoven
The Netherlands

ABSTRACT: This contribution deals with the application of computational homogenization techniques for structural masonry computations, as an alternative to the formulation of complex closed-form macroscopic constitutive laws. The complexity of modeling masonry material stems from the anisotropy evolution and localization induced by mesostructural damage. This phenomenon appears with preferential damage orientations, which are intimately related to the initial periodic structure of the material. The upscaling procedure used here relies on the formulation of mesoscopic constitutive laws at the level of the individual brick and mortar materials. A mesostructural unit cell with its corresponding periodicity requirements is used to deduce the average response of the masonry material through a scale transition. At the macroscopic scale, this averaged material response is used in the frame of an enhanced continuum approach with embedded localization bands, the widths of which are directly deduced from the initial periodicity of the material. The results obtained by the framework are illustrated and discussed by means of a structural computation example, which involves a complex cracking evolution together with fully anisotropic damage development.

KEY WORDS: masonry, computational homogenization, structural analysis, damage mechanics.

*Author to whom correspondence should be addressed. E-mail: thmassar@smc.ulb.ac.be
Figures 2, 3 and 11–15 appear in color online: http://ijd.sagepub.com

1056-7895/07/02 0199–28 $10.00/0 DOI: 10.1177/1056789506064943

INTRODUCTION

INCREASINGLY ADVANCED TECHNIQUES are nowadays used in structural rehabilitation of historical masonry structures. Numerical methods may be used for the analysis of such structures if they are able to account realistically for the possible failure modes of the masonry material, which strongly depend on the properties of its constituents, i.e., of the bricks and mortar. The nature of these quasi-brittle constituents, together with their geometrical arrangement, lead to the appearance of complex macroscopic responses (Dhanasekar et al., 1985). In the averaged behavior, the localization associated to intrinsic softening and interaction between initial orthotropy and damage-induced anisotropy are typical results thereof. The formulation of closed-form constitutive relations, which account for such mechanical effects is complicated, and strong assumptions are therefore often required in order to render such frameworks tractable. Furthermore, their experimental identification is mostly troublesome. The experimental work of Page and co-workers (Page, 1981, 1983; Dhanasekar et al., 1985), however, inspired several authors in the elaboration of such macroscopic phenomenological models intended for structural computations (Lourenço et al., 1997; Papa and Nappi, 1997; Berto et al., 2002). They tacitly assume that the experimental failure envelope shape obtained under proportional loading remains valid throughout the failure process for proportional as well as nonproportional loading. Furthermore, it is often assumed that the damaged material remains orthotropic. In reality, however, the response is highly path-dependent and the initial orthotropy of the initial material is generally lost through the development of asymmetric damage patterns (Dhanasekar et al., 1985; Massart et al., 2004).

Despite the intensive research dedicated to this field, the representation of general damage-induced anisotropy effects by means of closed-form constitutive laws remains far from established, even for initially isotropic materials. Existing frameworks accounting for cracking-induced anisotropy make use of tensorial damage variables of order two for orthotropic damage or of higher order for a more complex anisotropy evolution. This results in elegant but complex frameworks, featuring large numbers of parameters and/or model relations (Cormery, 1994; Govindjee et al., 1995; Halm, 1997; Carol et al., 2000a, b; Halm et al., 2002; Dragon, 2000). The identification of material-specific relations and parameters in such models poses a substantial difficulty, which is to be repeated for each new geometrical configuration of the constituents. Overcoming this problem by means of a computational homogenization scheme is the first goal of this study. Constitutive modeling is then limited to the level of individual constituents only, independent of their geometrical stacking.

The quasi-brittle nature of the constituent materials requires models which reflect the interplay between several length scales in the damaging process. The application of standard, local mechanical descriptions to cracking in quasi-brittle materials indeed leads to a loss of ellipticity of the equilibrium problem causing loss of well-posedness. Spurious mesh sensitivity and convergence toward physically nonadmissible solutions are the numerical outcomes. Therefore, higher-order frameworks have been introduced (de Borst et al., 1993). Most macroscopic models are, however, still formulated in terms of standard, first-order continua and do not include intrinsic length scale parameters. Instead, they often use the so-called crack band approach in order to reduce the pathological influence of the mesh size (Bažant and Planas, 1998). To avoid the problems associated with local models, some nonlocality may be introduced to approximate the response in the damage process zone, thereby introducing a material intrinsic length scale (Bažant, 1990; Bažant and Planas, 1998; Peerlings et al., 2001). With this type of approach, the discretization used for the solution of equilibrium boundary value problems is, however, strongly constrained by the width of the damage process zone. This raises serious difficulties if the typical size of the process zone is an order of magnitude smaller than the discretization size. This is often the case for masonry computations, where damage often propagates along the mortar joints. Furthermore, the introduction of an intrinsic length scale is more complex in an anisotropy setting, as this length parameter should reflect the anisotropic structure of the material. In such circumstances, one should resort to other approaches based on the introduction of displacement or strain discontinuities into which the material non-linearity is lumped, while the bulk of the material remains elastic (Sluys and Berends, 1998; de Borst, et al., 2001; Wells, 2001; de Borst, 2003).

As an alternative to current structural modeling approaches, the aim of this study is to illustrate the use of a strategy in which both the structural scale and the scale of constituents are integrated and interacting. The response in the damage process zone is described by a fine scale (mesostructural) description, while macrocracking is resolved at a coarse (structural) scale. This can be achieved by multiscale computational approaches proposed earlier (Feyel and Chaboche, 2000; Kouznetsova et al., 2001). It is postulated that the structural failure process is dominated by the material behavior at the scale of the constituents and by their geometrical arrangement. Isotropic phenomenological constitutive formulations are used at the level of these constituents, i.e., at the fine scale. The complexity of the overall behavior of masonry is naturally accounted for by a scale transition linking this fine scale description to the coarse scale. Since the process zone is several orders of magnitude smaller

than the structural scale, a discrete modeling strategy is used at the structural (coarse) scale, based on embedded weak discontinuities.

In this article, the emphasis is put on the motivation for using a classical macroscopic continuum description enhanced with embedded discrete bands for the failure behavior of masonry, in relation with the extraction of the average material response by means of computational homogenization techniques. Modified constituents laws are also introduced with respect to previous developments for the behavior of mortar joints. Finally, in contrast with other publications (Massart et al., 2006), a structural computation example is given here, in which the representation of full damage-induced anisotropy effects is a required feature to represent properly the energy dissipation.

This contribution is structured as follows. In the next section, the computational periodic homogenization technique is briefly recalled. The mesoscopic constitutive setting used for the constituents, based on continuum damage mechanics, is presented in section 'Mesoscopic constitutive setting'. The damage criterion used for the mortar constituent in previous papers is adapted here to improve its shape in the multiaxial compressive range. The use of computational homogenization to set up a coupled multiscale scheme for masonry is presented in section 'Upscaling procedure for damaging heterogeneous material'. The standard upscaling schemes require enhancements to represent localized material responses for quasi-brittle materials, which are commented upon. The key motivation for using a discrete localization band approach at the coarse scale upon localization detection is detailed in this section. Finally, the shear wall structural application is given in section 'Application' in order to illustrate the added value of the framework, on the basis of mesostructural damage patterns.

COMPUTATIONAL HOMOGENIZATION

In the frame of the periodic homogenization theory (Anthoine, 1995; Cecchi and Sab, 2002), the mesostructure of masonry and the loading applied to it are assumed to be periodic in the plane of the wall. A unit cell from which a fully homogeneously loaded wall can be rebuilt can be defined as the smallest periodic sample of the material. For a running bond stacking, it consists of one brick surrounded by half a mortar joint as illustrated in Figure 1. The periodic mesostructure of the material is reflected in the decomposition of the cell boundary into couples of segments which must fit together upon geometrical stacking of the cell. For a running bond stacking this boundary is split into six parts, tied two

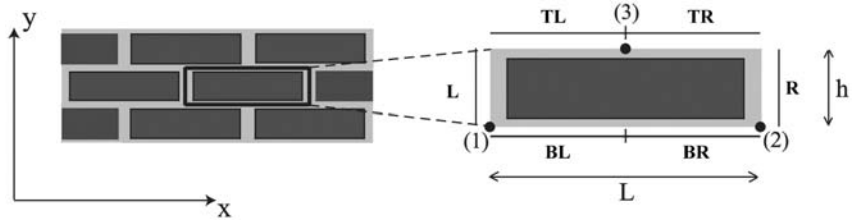

Figure 1. *Unit cell definition for running bond masonry. (L–R), (BL–TR), and (BR–TL) are homologous boundary segments, and numbers indicate controlling points.*

by two as sketched in Figure 1. The displacement field is assumed to have the form

$$\boldsymbol{u} = \mathbf{E} \cdot \boldsymbol{x} + \boldsymbol{w} \tag{1}$$

where $\mathbf{E}$ is the coarse scale strain tensor, $\boldsymbol{x}$ is the position vector of an arbitrary point within the cell and $\boldsymbol{w}$ is a mesoscopic fluctuation field which is added to the linear displacement field to account for the heterogeneity of the material. The macroscopic strain tensor may be computed as the volume average of the mesoscopic strain tensor

$$\frac{1}{V_{\text{cell}}} \int_{V_{\text{cell}}} \boldsymbol{\varepsilon}(\boldsymbol{u}) \mathrm{d}V = \mathbf{E} + \frac{1}{V_{\text{cell}}} \int_{S_{\text{cell}}} (\boldsymbol{w}\boldsymbol{n})^{\text{sym}} \, \mathrm{d}S_{\text{cell}} \tag{2}$$

where V_{cell} indicates the cell volume, and where $\boldsymbol{w}\boldsymbol{n}$ denotes the outer or dyadic product of vectors $\boldsymbol{w}$ and $\boldsymbol{n}$. If the fluctuation $\boldsymbol{w}$ is forced to be periodic (in the sense defined previously) on the cell boundary, the last integral vanishes due to the antiperiodicity of $\boldsymbol{n}$ on the coupled boundary segments. As a result, the macroscopic strain $\mathbf{E}$ is the average of the mesoscopic strain field. Practically, one has to enforce that the shape and orientation of homologous boundaries remain the same during the deformation process. This may be achieved for the unit cell represented in Figure 1 by means of the kinematical tying relations

$$\begin{aligned} \boldsymbol{u}_R &= \boldsymbol{u}_L + \boldsymbol{u}_2 - \boldsymbol{u}_1 \\ \boldsymbol{u}_{TR} &= \boldsymbol{u}_{BL} + \boldsymbol{u}_3 - \boldsymbol{u}_1 \\ \boldsymbol{u}_{TL} &= \boldsymbol{u}_{BR} + \boldsymbol{u}_3 - \boldsymbol{u}_2 \end{aligned} \tag{3}$$

where the subscripts refer to the boundary segments and controlling points as indicated in Figure 1. These relations also imply that the fluctuation field

is assumed to take identical values at the controlling points (1–3). The macroscopic strain tensor is then fully determined by the displacements of the three controlling points denoted by numbers 1–3 in Figure 1. The kinematics of the controlling points are related to the macroscopic displacement gradient components $\left(U_{,x}, U_{,y}, V_{,x}, V_{,y}\right)$ (i.e., the components of the macroscopic strain tensor) according to

$$\begin{aligned} u_1 &= 0 \\ v_1 &= 0 \\ u_2 &= LU_{,x} \\ v_2 &= LV_{,x} \\ u_3 &= hU_{,y} + \frac{L}{2}U_{,x} \\ v_3 &= hV_{,y} + \frac{L}{2}V_{,x} \end{aligned} \tag{4}$$

with L and h the length and the thickness of the cell respectively. The work equivalence principle (Hill-Mandel) is used in order to link the mesoscopic and macroscopic virtual works (Anthoine, 1995)

$$\boldsymbol{\Sigma} : \delta\mathbf{E} = \frac{1}{V_{\text{cell}}} \int_{V_{\text{cell}}} \boldsymbol{\sigma} : \delta\boldsymbol{\varepsilon} \, \mathrm{d}V \tag{5}$$

where $\delta\boldsymbol{w}$ is assumed periodic in the same sense as $\boldsymbol{w}$, which results in the expression of the macroscopic stress $\boldsymbol{\Sigma}$ as the average of the mesoscopic stress field

$$\boldsymbol{\Sigma} = \frac{1}{V_{\text{cell}}} \int_{V_{\text{cell}}} \boldsymbol{\sigma} \, \mathrm{d}V \tag{6}$$

Using mesoscopic equilibrium and Gauss' theorem, the macroscopic stress tensor may be expressed in terms of boundary quantities as

$$\boldsymbol{\Sigma} = \frac{1}{V_{\text{cell}}} \int_{V_{\text{cell}}} \boldsymbol{\sigma} \, \mathrm{d}V = \frac{1}{V_{\text{cell}}} \int_{S_{\text{cell}}} (\boldsymbol{t}\boldsymbol{x})^{\text{sym}} \, \mathrm{d}S_{\text{cell}} \tag{7}$$

where $\boldsymbol{t}$ is the traction vector acting in a point of the boundary S_{cell} of the unit cell and $\boldsymbol{x}$ is the position vector of such a point. Upon discretization in a finite element setting, each tying relation (3) between points of homologous

boundaries is associated with tying forces at the considered points and at the two involved controlling points. By expressing that these tying forces do not add extra virtual work to the system, combined with the periodicity tyings (3), it is possible to establish the relations between these tying forces, showing that they are antiperiodic at the boundary points and at the controlling points of the unit cell. As a result, it can be shown that the contribution in (7) of all these tying forces (including the tying forces at the controlling points) cancel each other (Kouznetsova et al., 2001; Geers, 2005). The average macroscopic stress is then obtained from the forces acting externally on the controlling points resulting from the action of neighboring cells $\boldsymbol{f}^{(i)}$ ($\boldsymbol{x}^{(i)}$ is the position of the controlling point (i) within the cell)

$$\boldsymbol{\Sigma} = \frac{1}{V_{cell}} \sum_{i=1}^{3} \boldsymbol{x}^{(i)} \boldsymbol{f}^{(i)} \tag{8}$$

MESOSCOPIC CONSTITUTIVE SETTING

Fine Scale Modeling Assumptions

The mechanical behavior of masonry is determined by a large number of factors. At the mesoscopic scale, the failure of masonry is governed by complex phenomena, i.e., failure of each of the constituents and of the interface between them. Since the focus in this contribution is set on the extraction of macroscopic behavior features based on a finer scale description, considerable simplifying assumptions will be introduced for the choice of a fine scale phenomenological description. The collective response of the mortar joints with the brick–mortar interfaces is frequently represented with cohesive surface elements (Lourenço and Rots, 1997). This type of formulation leads to effective computations, with a possibility for independent mode I and mode II responses. However, these approaches can induce difficulties, as stress oscillations are often observed which may hinder upscaling transitions. Furthermore, geometrical corrections are needed to account for the real geometry of the constituents. To avoid this type of problem, the fine scale modeling will be based on a continuum approach for both constituents. In contrast with the cohesive surface approach, this allows to incorporate the Poisson effect in the mortar joints, to account for the real dimensions of bricks and joints, and to obtain a better description of cracking evolution from head to bed joints. The physical interface between both constituents is assumed to be perfect and its failure is thus not explicitly

taken into account. Its effect on the average behavior is, however, incorporated by a modification of the tensile properties of mortar, such that they represent the tensile bond strength. Each individual constituent is assumed to be isotropic, assuming that the geometrical arrangement of the constituents is mainly responsible for the macroscopic induced anisotropy effects.

Implicit Gradient Damage Model

A strain-based implicit gradient damage model (Peerlings et al., 1996) is used to model both the brick and the mortar material at the mesoscopic scale. This model uses a scalar damage variable D, which enters the stress–strain relationship according to

$$\boldsymbol{\sigma} = (1 - D)\ {}^4\mathbf{L}_m : \boldsymbol{\varepsilon} \tag{9}$$

where ${}^4\mathbf{L}_m$ is the standard isotropic elasticity tensor. A damage criterion allows determination of whether a strain state change is accompanied by further damage

$$f(\overline{\varepsilon}_{eq}, \kappa) = \overline{\varepsilon}_{eq} - \kappa \leq 0 \tag{10}$$

along with the set of Kuhn–Tucker relations and an initial condition

$$f \leq 0 \quad \dot{\kappa} \geq 0 \quad f\dot{\kappa} = 0 \quad \kappa(t = 0) = \kappa_i \tag{11}$$

where κ represents the ultimate nonlocal equivalent strain state experienced by the material point in its loading history, constrained to be equal or larger than the initial value κ_i; and $\overline{\varepsilon}_{\mathrm{eq}}$ is a nonlocal equivalent strain introduced as the solution of a partial differential (averaging) equation incorporating a material intrinsic length scale l_c in the constitutive setting (Peerlings et al., 2001):

$$\overline{\varepsilon}_{\mathrm{eq}} - l_c^2 \nabla^2 \overline{\varepsilon}_{\mathrm{eq}} = \varepsilon_{\mathrm{eq}} \tag{12}$$

The smoothing of the field ε_{eq} obtained through equation (12) is similar to the one obtained with the nonlocal approach of the integral type as introduced in Pijaudier-Cabot and Bažant (1987). However, this smoothing is obtained by solving a single partial differential equation (Equation (12)) on the cell, rather than by computing a weighted spatial average in every point of interest as in Pijaudier-Cabot and Bažant (1987). The right-hand side in (12) is the source term for the nonlocal averaging, i.e., ε_{eq}, which is a

local equivalent scalar measure of the tensorial strain state. This partial differential equation is complemented by a natural boundary condition on the normal derivative of the nonlocal strain field at the boundary

$$\nabla \overline{\varepsilon}_{\text{eq}} \cdot \boldsymbol{n} = 0 \tag{13}$$

Classically, this boundary condition is applied at the free surface of the considered body. In the present case, the nonlocal averaged field is assumed to satisfy periodicity requirements which match those imposed on the other mechanical fields at the boundary of the unit cell, namely (Figure 1)

$$\begin{aligned} \overline{\varepsilon}_{\text{eq},\,R} &= \overline{\varepsilon}_{\text{eq},\,L} \\ \overline{\varepsilon}_{\text{eq},\,TR} &= \overline{\varepsilon}_{\text{eq},\,BL} \\ \overline{\varepsilon}_{\text{eq},\,TL} &= \overline{\varepsilon}_{\text{eq},\,BR} \end{aligned} \tag{14}$$

The boundary condition (13) is however applied inside the cell at the interface between dissimilar materials (the mortar and the brick). As shown in Peerlings et al. (2004), Equation (13) can be interpreted as an insulation condition between these materials as far as nonlocality is concerned. A damage evolution law relates the value of the damage D to the most severe nonlocal strain experienced by the material, κ. Details related to the implementation of the implicit gradient damage model using a finite element discretization are available in Peerlings et al. (1996). This type of model together with the proposed homogenization scheme was shown to capture qualitatively the load bearing capacity of masonry, and to give a good indication of the damage-induced anisotropy (Massart et al., 2004) including the failure mode (Anthoine, 1997; Massart et al., 2005b).

Damage Criteria for Constituents

The formulation of the damage model requires the definition of the scalar equivalent strain ε_{eq} for each of the constituents. For the brick material, the equivalent strain is defined in terms of the principal effective stresses by

$$\varepsilon_{\text{eq}} = \max_i \left(\frac{\langle \tilde{\sigma}_i \rangle}{E}, \frac{\langle -\tilde{\sigma}_i \rangle}{kE} \right) \tag{15}$$

where $\tilde{\sigma}_i$ are the principal values of the effective stress tensor $\tilde{\boldsymbol{\sigma}} = {}^4\mathbf{L}_m : \boldsymbol{\varepsilon}$ and k represents the ratio compressive strength/tensile strength for the brick material. The Macaulay brackets $\langle . \rangle$ are defined as $\langle x \rangle = 1/2(x + |x|)$.

For the combined effect of mortar and brick–mortar interface, a multilinear criterion is used in the space of the first two stress tensor invariants, denoted 'I_1^σ, J_2^σ' and is then translated into strain space in terms of the strain tensor invariants

$$I_1^\varepsilon = \varepsilon_{ii} \quad J_2^\varepsilon = \frac{1}{6} I_1^2 - \frac{1}{2}\varepsilon_{ij}\varepsilon_{ij} \tag{16}$$

Each segment is defined by the strength of the material for two specific loading cases. The equivalent strain is obtained by translating the criterion into strain space. A given segment i is given by

$$\varepsilon_{\mathrm{eq},\,i} = A_i \frac{I_1^\varepsilon}{(1-2\nu)} + B_i \frac{\sqrt{J_2^\varepsilon}}{(1+\nu)} \quad i = 1, \ldots, 4 \tag{17}$$

where the coefficients A_i, B_i are computed to match the experimental strength data related to the segment. The parameters used are $f_\mathrm{t}, f_\mathrm{c}, f_\mathrm{s}, f_\mathrm{b}$ and f_h, representing respectively the joint strength in uniaxial tension, uniaxial compression, biaxial compression under medium confinement (one principal stress half of the major one), triaxial compression under medium confinement (two principal stresses half of the major one), and hydrostatic compression. The shape of this criterion in the space of invariants of the stress tensor is illustrated in Figure 2 for the material parameters used in the computations, see Table 1. The criterion is much more sensitive in tension than in compression. Its shape is qualitatively similar to the failure surface used in Comi (2001) for concrete. It therefore yields a better description of the compressive behavior of the material under low to medium confinement than the criterion used hitherto (Massart et al., 2005b). Its shape in the principal stress space is illustrated in Figure 3 for the material parameters used in the computations and for the case of plane stress. Note that a

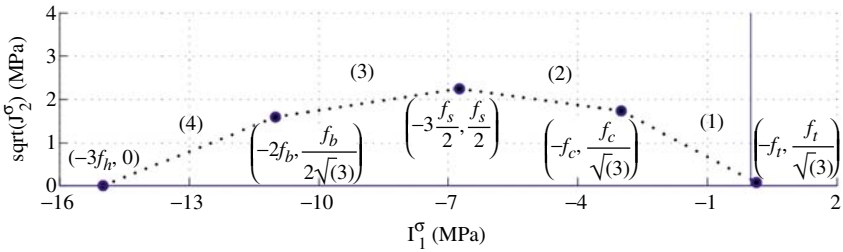

Figure 2. *Shape of the mortar damage loading surface in the stress invariants space. The five points controlling the criterion shape are defined by the five strength parameters as indicated in the figure.*

Table 1. Material parameters (values with * are typical values obtained from various sources in the literature (Page, 1981, 1983; Dhanasekara et al., 1985; van der Pluijm, 1999; Rots, 1997)). The multiaxial compressive strength parameters were chosen to yield a plane stress criterion shape comparable to concrete, see Comi (2001) and Figure 3.

Material	E (MPa)	ν	l_c (mm)	f_t (MPa)	β	f_c (MPa)	f_s (MPa)	f_b (MPa)	f_h (MPa)
Brick	16700*	0.15*	1.73	0.75	800*	15*	–	–	–
Mortar	3900*	0.20*	1.73	0.13*	85	3.0*	4.5	5.5	5.0

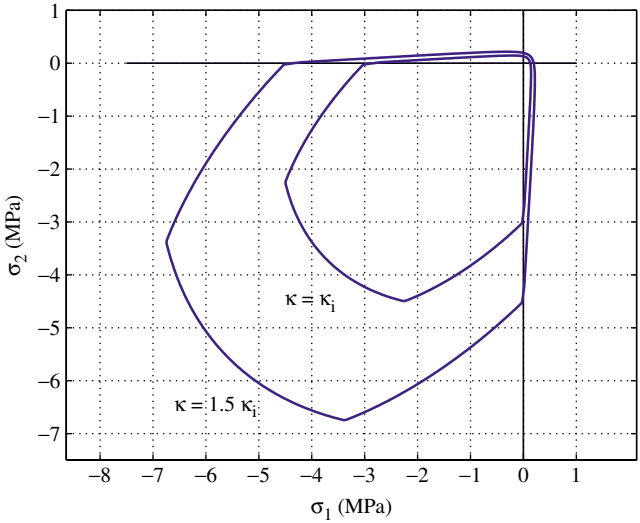

Figure 3. *Shape of the mortar damage loading surface in principal stress space (plane stress).*

generalised plane state assumption as described in Anthoine (1997) and Massart et al. (2005) will be used in 'Application' section, rather than a plane stress description.

An exponential damage evolution law is used to quantify damage growth

$$D = 1 - \frac{\kappa_i}{\kappa}\, e^{-\beta(\kappa - \kappa_i)} \tag{18}$$

The equivalent strain expressions (15) and (17) are defined such that damage is initiated when they reach the initial threshold value κ_i. The parameter β allows control of the softening tail of the stress–strain relation and is essentially related to the tensile fracture energy of the material. The material parameters used in the simulations are summarized in Table 1.

UPSCALING PROCEDURE FOR DAMAGING HETEROGENEOUS MATERIAL

Standard Continuous–Continuous Upscaling Procedure

NESTED MULTISCALE SCHEME

The multiscale computational scheme is based on the extraction of the average material behavior from a detailed representation at a finer scale using the homogenization principles explained in section 'Computational homogenization'. The standard multiscale approach (Feyel and Chaboche, 2000; Kouznetsova et al., 2001) is illustrated in Figure 4, and relies on a continuum description at the coarse scale, to be incorporated in the finite element solution scheme. A macroscopic strain $\mathbf{E}$ is obtained in each iteration of the macroscopic nonlinear solution procedure for all macroscopic sampling points (Gauss points). It is transferred to the finer scale by applying it to a representative volume element (restricted to a unit cell in this case) in an average sense, based on relations (1) and (2). The response of the representative volume element is obtained as the solution of an equilibrium problem at the fine scale, which furnishes the mechanical fields at the mesoscopic scale. The boundary value problem to be solved at the fine scale consists of the standard equilibrium equation $\nabla \cdot \boldsymbol{\sigma} = \mathbf{0}$, together with equations (9)–(13) introducing the nonlocality at this scale, and with the damage evolution laws (15)–(18) of the constituents. The boundary conditions are based on the averaging theorems and implemented via relations (3), (4), and (14), in which $\mathbf{E}$ is obtained from the coarse scale

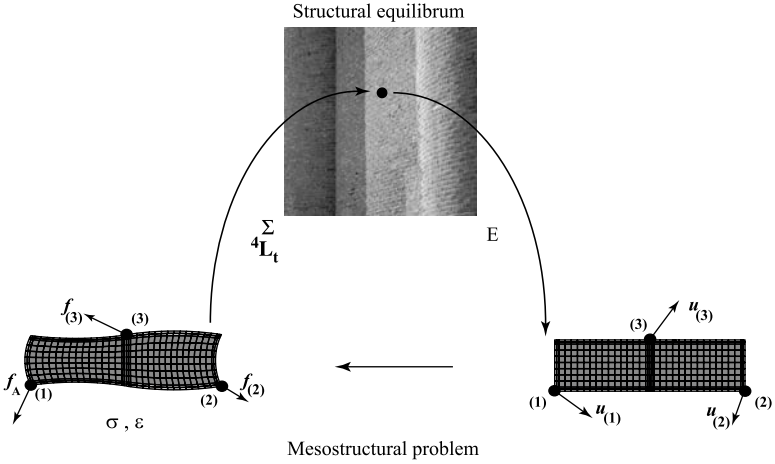

Figure 4. *Principle of first-order multiscale solution scheme.*

solution procedure and $\boldsymbol{w}$ and $\bar{\varepsilon}_{\text{eq}}$ are forced to be periodic at cell the boundary. Based on the solution of this fine scale problem, the macroscopic stress $\boldsymbol{\Sigma}$ is then computed by averaging the mesoscopic stress field $\boldsymbol{\sigma}$ with relation (8). The scale transition also permits extraction of the coarse scale or macroscopic constitutive tangent ${}^4\mathbf{L}_{\text{M}}$, which relates variations of $\boldsymbol{\Sigma}$ to variations of $\mathbf{E}$, by static condensation of the discrete fine scale tangent stiffness (Kouznetsova et al., 2001). After convergence at the fine scale, its condensation to the controlling points reads

$$\sum_{p=1}^{3} \mathbf{K}_M^{(np)} \cdot \delta \boldsymbol{u}^{(p)} = \delta \boldsymbol{f}^{(n)}, \quad n = 1, 2, 3 \tag{19}$$

where $\mathbf{K}_M^{(np)}$ is a second-order tensor relating the variation of the displacement vector of controlling point (p) to the variations of the mesoscopic force vector at controlling point (n). Substituting relation (19) in the variation of (8), and making use of (1) yields

$$\delta \boldsymbol{\Sigma} = \underbrace{\left(\sum_{n=1}^{3} \sum_{p=1}^{3} \boldsymbol{x}^{(n)} \mathbf{K}_M^{(np)} \boldsymbol{x}^{(p)} \right)^{(rs)}}_{{}^4\mathbf{L}_{\text{M}}} : \delta \mathbf{E} \tag{20}$$

where $(\cdot)^{(rs)}$ denotes that right symmetry of the homogenised stiffness has been taken into account, and $\boldsymbol{x}^{(p)}$ denotes the position vector of controlling point (p).

It is noted that the standard continuous–continuous upscaling procedure recalled here is based on the assumption that a sufficient scale separation exists between the selected fine scale and coarse scale descriptions. This hypothesis is indeed implicitly introduced by the use of a standard (first order) continuum description at the coarse scale, and is reflected in the periodicity assumption introduced in (1), (2).

CHOICE OF THE REPRESENTATIVE VOLUME ELEMENT

In a general context, the choice of the size of the representative volume element is an important issue since it influences the extracted average response, especially for disordered materials. In the present case of periodic boundary conditions, and since the mesostructure of masonry is periodic, a unit cell (i.e., a single period representative volume element) is sufficient, as long as the extracted average response remains unique. Since geometrical linearity is assumed, loss of uniqueness in the average response of the representative volume element is not size-dependent and is caused by loss of

ellipticity due to the material nonlinearity (damage) (Massart et al., 2004). A similar analysis with a larger periodic representative volume element would only deviate from the unit cell computation when loss of uniqueness occurs. From this point, the macroscopic response may switch to a localised deformation mode, which has to be dealt with. As a result, the validity of the standard continuous–continuous approach is further restricted. The purpose of the following sections is to propose a methodology to represent the subsequent localised behavior by including discrete localization bands in the structural scale description.

Localisation Enhanced Continuous–discontinuous Upscaling Procedure

MASONRY FAILURE AND LOCALIZATION

Local constitutive theories notoriously suffer from pathological localization when used to model damage and fracture (de Borst et al., 1993). A number of approaches have been proposed in order to enhance continuum formulations by including an intrinsic length parameter to avoid such deficiencies (de Borst et al., 1993; Peerlings et al., 1996). At the mesoscopic scale, a gradient damage model is used for this purpose (Peerlings et al., 1996).

At the coarse scale, a higher-order continuum approach is to be avoided as the damage process zone size is usually too small to be explicitly resolved at this scale. Instead, a discrete localization band is introduced, with a specific localization bandwidth which corresponds to the smallest possible period in the material structure along the localization orientation associated to each typical failure mechanism. This assumption is illustrated in Figure 5 for the case of a staircase crack pattern in running bond masonry.

The inclusion of embedded localization bands in the macroscopic description requires the definition of a traction-opening displacement relation which should be obtained from the fine scale description using

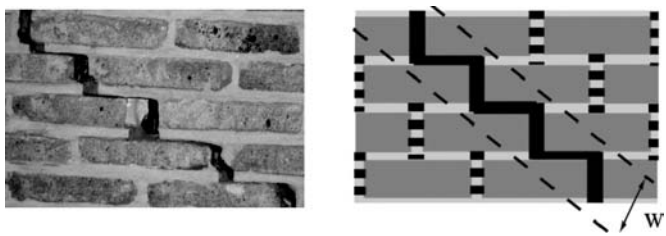

Figure 5. *Extraction of a localization bandwidth based on the stacking of the material: (left) real failure pattern, (right) localization bandwidth associated to the final failure pattern.*

computational homogenization techniques. The corresponding scale transition presents the following features:

- The bifurcation from a macroscopically homogeneous deformation state is assumed, giving rise to the appearance of a discrete localization band. Both the bifurcation point and the band orientation need to be detected from the upscaling procedure.
- The upscaling procedure should correctly transfer the amount of dissipated energy, and should therefore explicitly transfer to the coarse scale the volume (the bandwith) in which the fine scale dissipation occurs.
- As a result of the presence of a weaker quasi-brittle constituent (mortar) with a low volume fraction inside the mesostructural unit cell, snap-back effects may arise in the average response of a unit cell. The scale transition procedure should allow the control of the fine scale energy dissipation, thereby enabling path following at the unit cell level.
- Finally, a snap-back effect may also be present in the average response of an integration point of the coarse scale description. This effect may be induced by the presence of a softening thin band embedded in a finite-sized integration volume in the coarse scale description.

INCLUSION OF A STRAIN DISCONTINUITY AT THE COARSE SCALE

The structural scale problem (i.e., coarse scale) is solved using the finite element method and using an embedded band model in which the behavior of the band is obtained from fine scale computations. The failure process is taken into account at the coarse scale through the response of the integration points, without any enrichment of their kinematics. This choice allows use of a standard discretization scheme at the coarse scale, even though it is well known that it suffers from some drawbacks such as the lack of macrocrack path continuity and objectivity (Jirásek, 2000; Wells, 2001). The standard two-scale scheme described in section 'Standard continuous–continuous upscaling procedure' is used prior to localization, where the response of a unit cell is attributed to the finite volume associated with each coarse scale Gauss point. The damage evolution is completely controlled by the fine scale computations, which allows capture of complex anisotropy development at the coarse scale, a feature difficult to achieve with closed-form models. Upon damage propagation in the fine scale solution, the onset of localization is detected based on the appearance of negative eigenvalues of the homogenised tangent operator. Note that this is a sufficient but not a necessary condition; more details on this choice are available in Massart (2003). The orientation of the discrete band

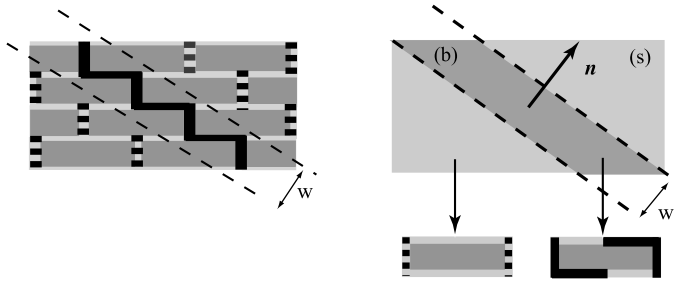

Figure 6. *Idealization of the constitutive response for a macroscopic material point. A unit cell is associated to each sub-region.*

of localization is obtained from an eigenspectrum analysis of the acoustic tensor, as introduced in Rice (1976) and Rice and Rudnicki (1980).

Once localization is detected at a coarse scale quadrature point, a band with a particular width has to be included in the associated volume. The bandwidth is prescribed by the geometry of the associated fine scale crack pattern, which is in turn closely related to the stacking mode of the constituents. The band is embedded by considering the integration volume as a two-phase material made of a damaging band surrounded by a (potentially damaged) elastically unloading phase, see Figure 6. The response of the damaging phase is extracted from the fine scale description by means of the standard upscaling procedure described previously. The same procedure is used to determine the unloading response of the surrounding material from a second unit cell which is now initialized, representing the elastic state of the material at the moment of bifurcation. The collective (averaged) response of the band and its surrounding is obtained from a relaxed Taylor assumption (Evers et al., 2002). A kinematically admissible strain jump is allowed to appear across the localization band. A uniform strain field is assumed in each phase, depending on the respective volume fractions of the band and surrounding $f^{\mathrm{b}}, f^{\mathrm{s}}$ and on the strain jump vector $\boldsymbol{m}$:

$$\begin{aligned} \mathbf{E}^{\mathrm{b}} &= \mathbf{E} + f^{\mathrm{s}}(\boldsymbol{m}\boldsymbol{n})^{\mathrm{sym}} \\ \mathbf{E}^{\mathrm{s}} &= \mathbf{E} - f^{\mathrm{b}}(\boldsymbol{m}\boldsymbol{n})^{\mathrm{sym}} \end{aligned} \tag{21}$$

Furthermore, continuity of tractions is required to hold at the interface between both phases

$$\boldsymbol{n}.\left(\delta\boldsymbol{\Sigma}^{\mathrm{b}} - \delta\boldsymbol{\Sigma}^{\mathrm{s}}\right) = \boldsymbol{0} \tag{22}$$

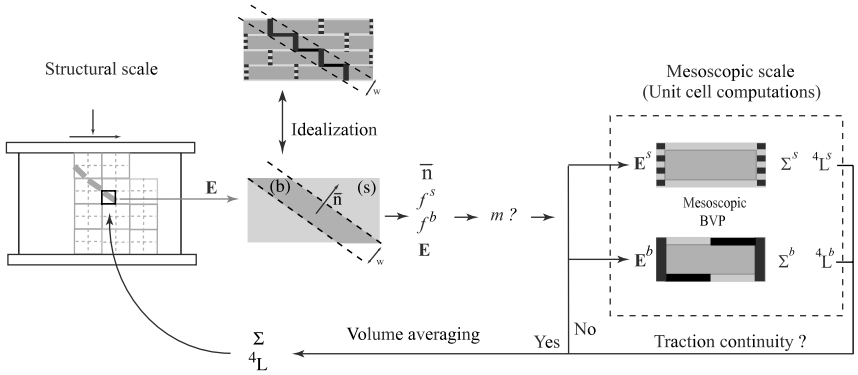

Figure 7. *Localization enhanced multiscale scheme with embedded strain discontinuities.*

The averaged response of this composite approximation is obtained by volume averaging of the stresses in both phases

$$\delta\boldsymbol{\Sigma} = f^{\mathrm{b}}\delta\boldsymbol{\Sigma}^{\mathrm{b}} + f^{\mathrm{s}}\delta\boldsymbol{\Sigma}^{\mathrm{s}} \tag{23}$$

Note that since the traction-opening displacement response of the band is nonlinear, Equation (22) has to be solved iteratively. The entire localization enhanced upscaling procedure is sketched in Figure 7.

DISSIPATION CONTROL FOR FINE SCALE SNAP-BACK EFFECTS

Due to the quasi-brittle nature of the constituents, snap-back may occur in the averaged response of an integration point at the structural scale, i.e., a decreasing strain may be predicted for continued (dissipative) loading of the material. This effect is intimately linked to the nonhomogeneous mechanical fields considered in a finite volume associated to the integration point. As a result, the size of the damage process zone in which energy is dissipated may well be small with respect to the unloading part of the material. The snap-back effect may arise as a result of the averaging procedures. It may appear in the relaxed Taylor model averaging (23) if the localization band width is small with respect to the coarse scale discretization, or in the damaging unit cell averaging (8) as localization may appear in the mortar joints which are thin with respect to the unit cell size. Note that these physically realistic effects are nonexisting in closed-form models at the coarse scale where integration points are assumed to represent homogeneously deformed infinitesimal volumes. These effects are linked to the incorporation of the finite size of the material constituents, which is a key feature of the presented approach.

The snap-back caused by the finite volume averaging at the coarse scale integration points (23) can be controlled by considering the strain jump $\boldsymbol{m}$ as an unknown of the coarse scale solution. A path following technique can then be constructed to seek for increasing values of the strain jump, thereby allowing to follow a dissipative response. Equation (22) which is conjugate to $\boldsymbol{m}$ is also shifted to the coarse scale solution procedure, associated to each integration point in which bifurcation into a localised state has occurred.

The potential snap-back in the average response of the damaging unit cell can be controlled through the fine scale nonlocal strain field $\overline{\varepsilon}_{\text{eq}}$ which drives damage growth at the fine scale. It is then possible to trace the fine scale snap-back path by requiring further dissipation at the fine scale. To achieve this, a properly selected mesoscopic fine scale nonlocal strain variable is shifted to the coarse scale solution procedure along with its conjugate nodal equation, requiring that the conjugate residual vanishes at equilibrium (i.e., no external macroscopic action on the unit cell to obtain the required dissipation at equilibrium).

More details related to the dissipation control used for the fine scale boundary value problem can be found in Massart et al. (2005a). The detailed theoretical and computational aspects of this two-scale model are provided in Massart (2003) and Massart et al. (2006), where the issues related to the branching procedure upon bifurcation detection and to the selection of the constraint to use for fine scale dissipation control are addressed.

OVERVIEW OF THE COMPLETE SCALE TRANSITION PROCEDURE

The complete two-scale solution strategy used for masonry structural computations is sketched in Figure 8, together with the set of equations solved at each scale. The decomposition of the coarse scale integration point behavior into a localizing band and its surrounding material is given, as well as the averaging of phase stresses resulting from the associated fine scale problems. The embedded band is defined by its orientation $\boldsymbol{n}$ and its strain jump $\boldsymbol{m}$.

The snap-back handling procedures require the incorporation of the strain jump and the controlling fine scale nonlocal strain unknowns in the coarse scale solution procedure. The damaging fine scale boundary value problem is constructed from the average strain in the band obtained from the coarse scale and the relaxed Taylor model. A procedure has to be defined to select the optimal nonlocal strain used to trace the snap-back path. The shifting of unknowns to the coarse scale is illustrated in Figure 8.

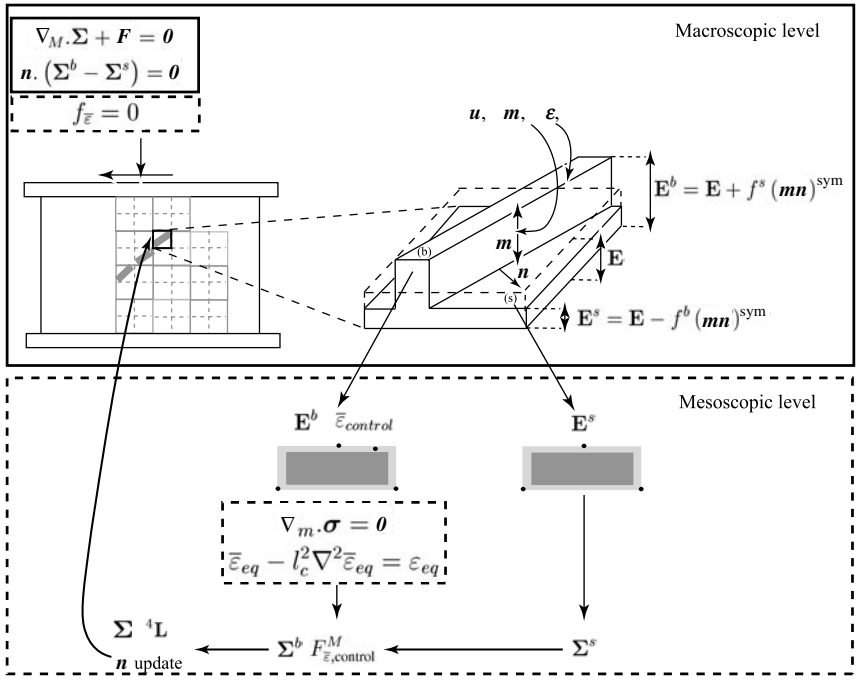

Figure 8. *Enhanced first-order multiscale scheme with embedded strain discontinuity for localized behavior and average material response snap-back handling.*

As mentioned in the previous paragraphs, static equilibrium is solved at the fine scale together with a nonlocal averaging equation (dashed lines). The (fine scale) residual equation conjugate to this nonlocal strain which is solved at the coarse scale level together with coarse scale equilibrium and with the traction continuity along the interface between the phases in the two-phase problem. This is emphasized in Figure 8 by the dashed lines surrounding this equation.

Note that the scale separation assumption alluded to in the section entitled 'Standard continuous-continuous upscaling procedure' for the standard upscaling procedure is still implicitly used in the localization enhanced model as well, because the coarse scale standard continuum description is used for the response prior to localization. As a result, the presented framework is mainly intended for large scale structural computations where a sufficient scale separation between the structural size and the unit cell is indeed observed.

APPLICATION

Confined Shearing of a Full Masonry Wall

Data related to large scale masonry tests is rather scarce in the literature. Raijmakers and Vermeltfoort (1992) performed experiments on shearing walls. These experiments were however performed on small scale structures made of a limited number of bricks. The scale jump in these experiments is rather small, for which the presented approach was not designed. A similar test with an increased scale jump however, is analyzed here to verify whether a qualitative agreement can be obtained in terms of the cracking evolution and of the resulting structural failure mode.

PROBLEM DESCRIPTION AND QUALITATIVE EXPERIMENTAL BEHAVIOR

The tested geometry is shown in Figure 9. It consists of a plane masonry wall of dimensions $3000 \times 3000 \times 100\,\text{mm}^3$. The clamping of the top and bottom boundaries of the wall in the loading set-up has been represented by two bands of elements with elastic behavior and with a stiffness comparable to concrete. The loading is applied in two phases. In the first phase, the wall is compressed by a vertical uniformly distributed load of 130 kN applied to the top beam, resulting in a uniform vertical displacement of the top boundary. In the second loading phase, the vertical displacement of the top boundary is kept fixed and a horizontal shearing force is applied. The average crack pattern orientations obtained experimentally are illustrated in

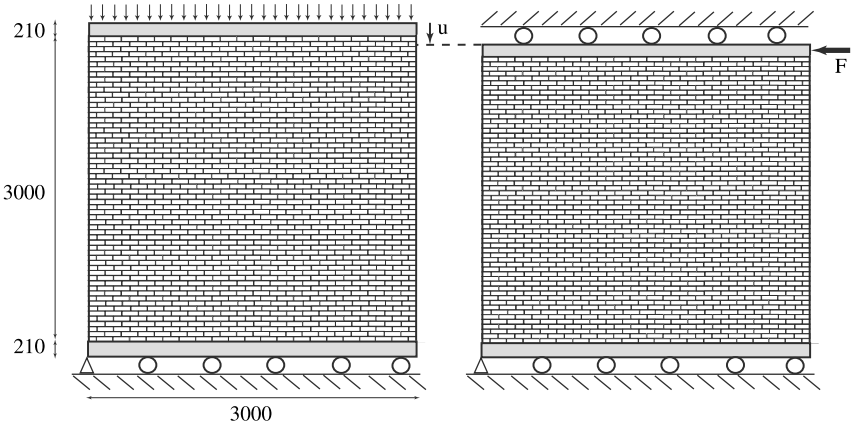

Figure 9. *Shear test on a masonry wall: two-phase loading and dimensions.*

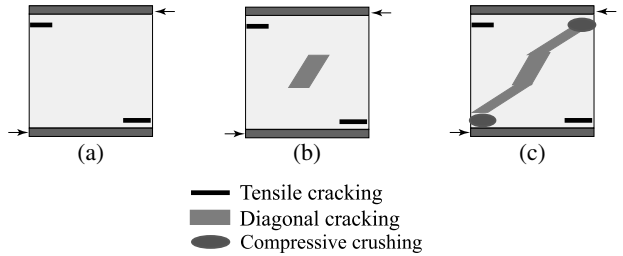

Figure 10. *Shear test on a full wall – cracking stages observed in experiments by (Raijmakers and Vermeltfoort).*

Figure 10 (Raijmakers and Vermeltfoort, 1992). The initiation of damage depends on the magnitude of the vertical compression load. For low precompression loads, damage is first initiated during the confined shearing phase with the appearance of horizontal tensile cracks at the top-left and bottom-right corners of the wall (Figure 10(a)). The extension of these tensile damage zones is slowed down by the initial compression. The appearance of these tensile cracking zones is followed by the formation of a compressive strut between the bottom left and top right corners. Upon further shearing, diagonal cracking appears in the central zone of the specimen in the compressive strut (Figure 10(b)). Finally, a structural failure mechanism is formed by the propagation of diagonal cracking toward the compressed corners of the wall (Figure 10(c)). Depending on the compressive strength of the mortar, final failure may occur by compressive crushing at the compressed corners of the wall, associated with brick cracking at the mesoscopic level.

For the numerical simulation, the mesostructure of the material is made of bricks of dimensions $140 \times 65 \times 100$ mm^3 with 10 mm thick mortar joints. The unit cell is discretized with a mesh of 396 elements with a biquadratic interpolation of the displacement field and a bilinear interpolation of the nonlocal strain field. A generalized plane state assumption is used at the mesoscopic scale (Massart et al., 2005b), and the material parameters of Table 1 are used for the constituents. At the macroscopic scale, an unstructured mesh of 114 triangular elements is used, with a linear displacement interpolation and a single integration point per element. The use of the multiscale framework with these discretizations requires the solution of 114 mesoscopic problems containing 2845 independent mesoscopic degrees of freedom each. Based on the ratio between structural and mesoscopic dimensions, a full fine scale modeling of this structure would require the solution of a structural equilibrium problem with more than three million degrees of freedom.

NUMERICAL RESULTS

The evolution of macroscopic localization during the computation is illustrated in Figures 11–15 by the emerging embedded localization bands and the mesoscopic damage in typical unit cells. As depicted in Figure 11, cracking is indeed initiated at the top-left and bottom-right corners of the wall. The orientation of the embedded localization bands is almost horizontal, due to vertical tensile stresses. At this stage, no damage is present in the central zone of the specimen as indicated by the middle unit cells depicted in Figure 11. Upon further shearing, diagonal cracking is initiated in the compressive strut (middle cell of Figure 12), due to the combined effect of macroscopic vertical compression and shearing. This stress state causes a staircase crack pattern to appear at the mesoscopic scale. This may be observed in the initiation of mesostructural cracking (Figure 12), but also in the orientation of macroscopic localization bands (Figure 13). Finally, the diagonal cracking further progresses. This extension of the cracking in the central compressive strut approximately matches the macroscopic shear distribution depicted in Figures 14 and 15.

This is reflected in the set of unit cells represented in Figures 14 and 15, where most fine scale damage patterns are oriented in a direction corresponding to a staircase pattern. The mesoscopic damage state of nonlocalized unit cells in Figures 14 and 15 show that damage ultimately tends to progress toward the bottom-left and top-right corners of the wall. Furthermore, the fine scale pattern also tends toward staircase cracking of

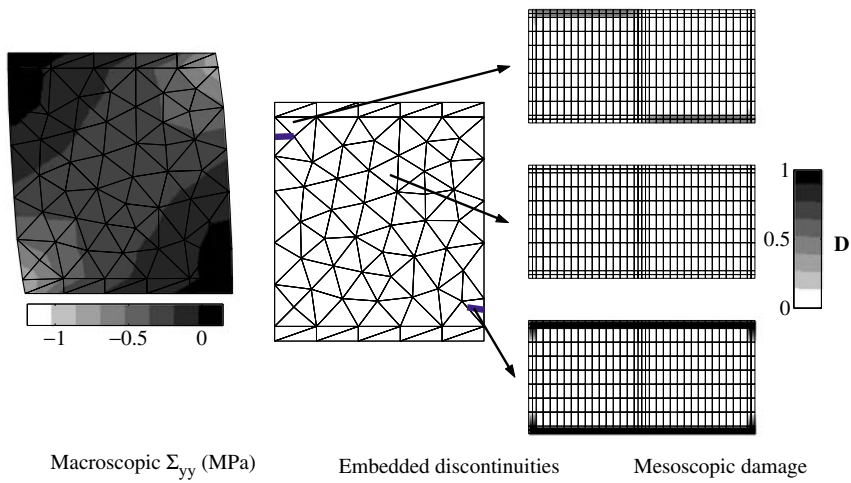

Figure 11. *Damage state at initiation of tensile cracking (shearing load $F = 93.3$ kN): (left) macroscopic vertical stress distribution responsible for tensile cracking, (center) embedded discontinuities and (right) mesoscopic damage states.*

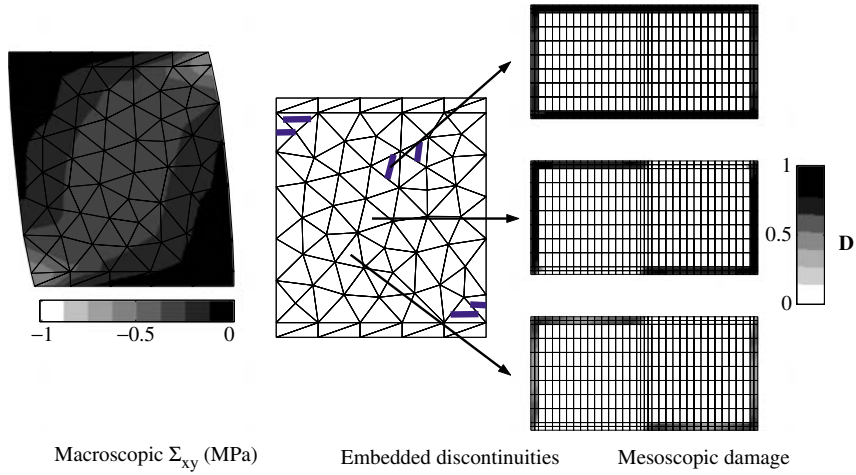

Figure 12. *Damage state upon initiation of diagonal cracking (shearing load F =129.9 kN): (left) macroscopic shearing stress distribution, (center) embedded discontinuities and (right) mesoscopic damage states.*

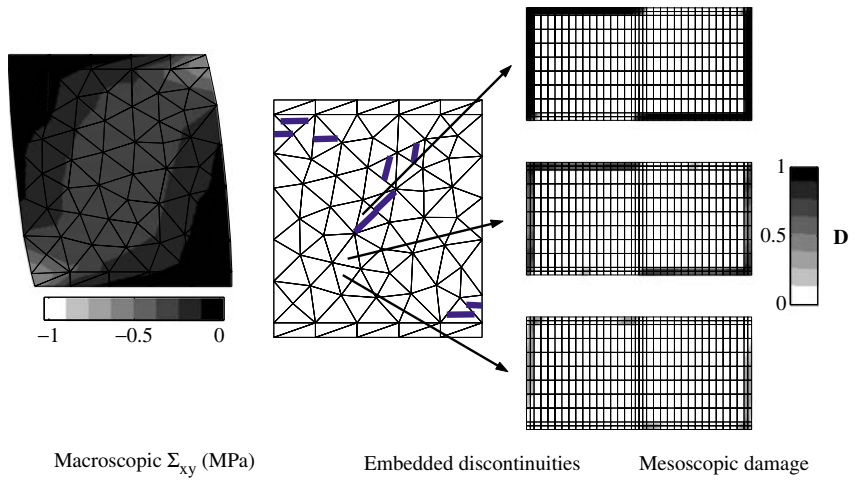

Figure 13. *Damage state for propagation of diagonal cracking (shearing load F =132 kN): (left) macroscopic shearing stress distribution, (center) embedded discontinuities and (right) mesoscopic damage states.*

joints near the compressed corners of the wall (top and bottom unit cell of Figure 15), or cracking of head joints (middle unit cell of Figure 15). From Figure 15, the structural failure mechanism can be well identified. The Figure 14 is obtained for a limit point of the structural load–displacement

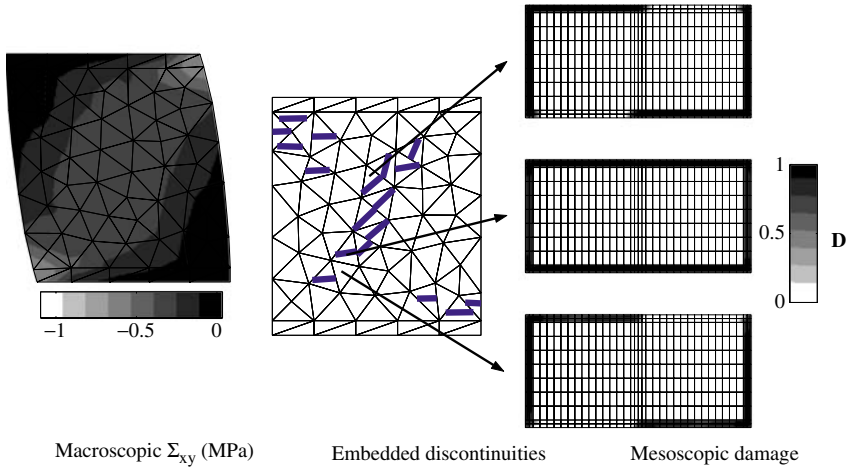

Figure 14. *Damage state for propagation of diagonal cracking (shearing load F =141 kN): (left) macroscopic shearing stress distribution, (center) embedded discontinuities and (right) mesoscopic damage states.*

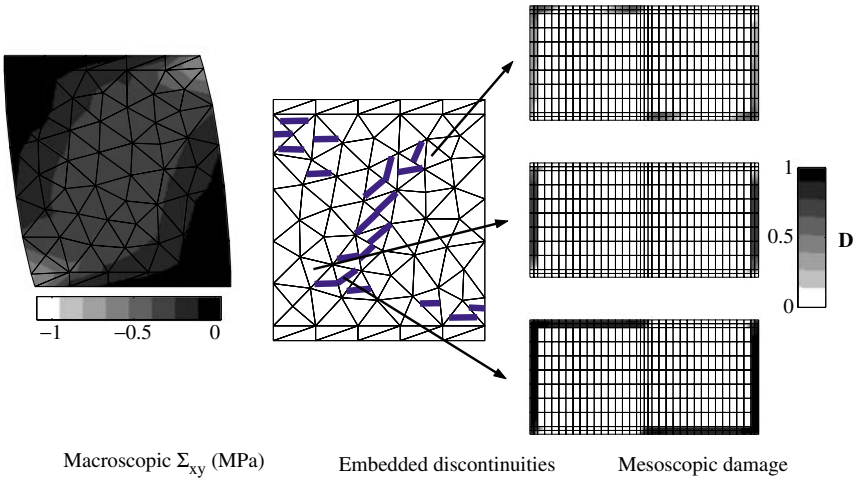

Figure 15. *Final damage state obtained for a shearing force F = 140.7 kN: (left) macroscopic shearing stress distribution, (center) embedded discontinuities and (right) mesoscopic damage states.*

response, but it is unknown whether this is a global limit point. The complete postpeak response has not been traced due to loss of convergence in some stage of the computations. Since the post-peak regime is not of practical relevance for most structural failure problems in masonry, no further attention is given to it here.

Nevertheless, this test illustrates that a structural damage analysis can be achieved based on tractable mesoscopic material parameters using multiscale techniques.

CONCLUSIONS

In this contribution, a localization enhanced multiscale modeling approach is applied for the simulation of cracking in plane masonry structures. In this framework, the material response is obtained from a unit cell by means of scale transitions, avoiding the formulation of complex macroscopic constitutive laws. As a result, complex cracking-induced anisotropy effects can be described, a unique feature of this type of model. The scale transitions are formulated in such a way that it is possible to handle snap-back effects in the averaged material response, which ensue from the quasi-brittle nature of the constituents. Localization of damage is represented using a macroscopic continuum approach enhanced with embedded localization bands. The appearance and the orientation of these localization bands is deduced from the unit cell computations. Their width is directly motivated from the initial periodic mesostructure of the material. It is shown in this article that the use of a discrete localization band model at the coarse scale allows modeling of the rather thin process zones (smaller than the typical fine scale unit cell) without the need to resolve them at the level of the coarse scale discretization. Fine scale constitutive laws similar to those used for concrete have been proposed to improve the response of the mortar material under multiaxial compression under low to medium confinement. Such modifications in mesostructural behavior features are naturally accommodated thanks to the flexibility of the upscaling procedure. A structural computational example has been given to illustrate the ability of the proposed approach to describe complex cracking evolution in masonry structures. As illustrated here, it is especially important when cracking-induced full anisotropy has to be taken into account. Again, it is emphasized that this feature is rarely included in existing structural scale approaches. Yet, for effective structural calculations, additional developments are still required in order to improve the framework. One of its main limitations resides in its high computational cost, linked to the triggering of fine scale computations for each coarse scale integration point, irrespective of the fact that its behavior can remain linear elastic. A considerable gain could, therefore, be obtained if criteria are formulated to detect if no damage evolution is present on the fine scale without computing explicitly the fine scale response. Secondly, the lack of crack path continuity at the coarse scale may alter the representation of energy dissipation when highly localized failure patterns appear at the coarse scale. Crack path continuity

would therefore improve the description for this type of failure. Finally, the formulation of a scale transition accounting for out-of-plane flexural effects would be needed for the simulation of complex structures.

ACKNOWLEDGMENTS

Fruitful discussions with Dr A. Anthoine related to the mesoscopic damage criteria used for constituents are gratefully acknowledged. The first author was partially supported financially by the Région Wallonne (Belgium) under grant 215089 (HOMERE).

REFERENCES

Anthoine, A. (1995). Derivation of the In-plane Elastic Characteristics of Masonry through Homogenisation Theory, *International Journal of Solids and Structures*, **32**(2):137–163.

Anthoine, A. (1997). Homogenization of Periodic Masonry: Plane Stress, Generalized Plane Strain or Three-dimensional Modelling?, *Communications in Numerical Methods in Engineering*, **13**: 319–326.

Bažant, Z.P. (1990). Why Continuum Damage is Nonlocal: Micromechanics Arguments, *Journal of Engineering Mechanics*, **117**(5): 1070–1087.

Bažant, Z.P. and Planas, J. (1998). Fracture and Size Effect in Concrete and other Quasi-brittle Materials, CRC Press, Boca Raton.

Berto, L., Saetta, A., Scotta, R. and Vitaliani, R. (2002). An Orthotropic Damage Model for Masonry Structures, *International Journal for Numerical Methods in Engineering*, **55**: 127–157.

Carol, I., Rizzi, E. and Willam, K. (2000a). On the Formulation of Anisotropic Elastic Degradation: Part I. Theory Based on a Pseudo-logarithmic Damage Tensor Rate, *International Journal of Solids and Structures*, **38**(4): 491–518.

Carol, I., Rizzi, E. and Willam, K. (2000b). On the Formulation of Anisotropic Elastic Degradation: Part II: Generalized Pseudo-Rankine Model for Tensile Damage, *International Journal of Solids and Structures*, **38**(4): 519–546.

Cecchi, A. and Sab, K. (2002). A Multiparameter Homogenisation Study for Modelling Elastic Masonry, *European Journal of Mechanics A/Solids*, **21**: 249–268.

Comi, C. (2001). A Non-local Model with Tension and Compression Damage Mechanisms, *European Journal of Mechanocs A/Solids*, **20**: 1–22.

Cormery, F. (1994). Contribution à la modélisation de l'endommagement par mésofissuration et du phénomène de localisation associé, PhD Thesis, Université de Poitiers (in French).

Dhanasekar, M., Page, A.W. and Kleeman, P.W. (1985). The Failure of Brick Masonry Under Biaxial Stresses, In: *Proc. Instn. Civ. Engrs., Part 2*, pp. 295–313.

Dragon, A. (2000). Continuum Damage Mechanics Applied to Quasi-brittle Materials, In: Allix, O. and Hild, F. (eds), *Damage Mechanics of Materials and Structures*, 165–203, LMT-ENS Cachan, Elsevier.

de Borst, R., Sluys, L.J., Muhlhaus, H.B. and Pamin, J. (1993). Fundamental Issues in Finite Element Analyses of Localisation of Deformation, *Engineering Computations*, **10**: 99–121.

de Borst, R., Wells, G.N. and Sluys, L.J. (2001). Some Observations on Embedded Discontinuity Models, *Engineering Computations*, **18**(1–2): 241–254.

de Borst, R. (2003). Numerical Aspects of Cohesive-zone Models, *Engineering Fracture Mechanics*, **70**(14): 1743–1757.

Evers, L.P., Parks, D.M., Brekelmans, W.A.M. and Geers, M.G.D. (2002). Crystal Plasticity Model with Enhanced Hardening by Geometrically Necessary Dislocation Accumulation, *Journal of the Mechanics and Physics of Solids*, **50**: 2403–2424.

Feyel, F., Chaboche, J.L. (2000). FE^2 Multiscale Approach for Modelling the Elastoviscoplastic Behavior of Long Fiber SiC/Ti Composite Materials, *Computer Methods in Applied Mechanics and Engineering*, **183**: 309–330.

Geers, M.G.D. (2005). Multiscale Modelling and Design of New Materials (Course Notes), *International Center for Mechanical Sciences*, Udine.

Govindjee, S., Kay, G.J. and Simo, J.C. (1995). Anisotropic Modelling and Numerical Simulation of Brittle Damage in Concrete, *International Journal for Numerical Methods in Engineering*, **38**: 3611–3633.

Halm, D. (1997). Contribution à la modélisation du comportement unilatéral et du frottement dans les matériaux mésofissurés, PhD Thesis, Université de Poitiers (in French).

Halm, D., Dragon, A. and Charles, Y. (2002). A Modular Damage Model for Quasi-brittle Solids – Interaction between Initial and Induced Anisotropy, *Archive of Applied Mechanics*, **72**: 498–510.

Jirásek, M. (2000). Comparative Study on Finite Elements with Embedded Discontinuities, *Computer Methods in Applied Mechanics and Engineering*, **188**: 307–330.

Kouznetsova, V.G., Brekelmans, W.A.M. and Baaijens, F.T.P. (2001). An Approach to Micro-macro Modelling of Heterogeneous Materials, *Computational Mechanics*, **27**: 37–48.

Lourenço, P.B. and Rots, J.G. (1997). Multi-surface Interface Model for Analysis of Masonry Structures, *Journal of Engineering Mechanics*, **127**(3): 272–280.

Lourenço, P.B., de Borst, R. and Rots, J.G. (1997). A Plane Stress Softening Plasticity Model for Orthotropic Materials, *International Journal for Numerical Methods in Engineering*, **40**(21): 4033–4057.

Massart, T.J. (2003). Multi-scale Modeling of Damage in Masonry Structures, PhD Thesis, Université Libre de Bruxelles & Eindhoven University of Technology.

Massart, T.J., Peerlings, R.H.J. and Geers, M.G.D. (2004). Mesoscopic Modeling of Failure and Damage-induced Anisotropy in Brick Masonry, *European Journal of Mechanics A/Solids*, **23**(5): 719–735.

Massart, T.J., Peerlings, R.H.J. and Geers, M.G.D. (2005a). A Dissipation-based Control Method for the Multi-scale Modelling of Quasi-brittle Materials, C.R. Mécanique (in press).

Massart, T.J., Peerlings, R.H.J., Geers, M.G.D. and Gottcheiner, S. (2005b). Mesoscopic Modeling of Failure in Brick Masonry Accounting for Three-dimensional Effects, *Engineering Fracture Mechanics*, **72**: 1238–1253.

Massart, T.J., Peerlings, R.H.J. and Geers, M.G.D. (2006). An Enhanced Multi-scale Approach for Masonry Walls Computations with Localisation of Damage – Part I. Concepts and Treatment of Localisation, Submitted for publication.

Massart, T.J., Peerlings, R.H.J. and Geers, M.G.D. (2006). An Enhanced Multi-scale Approach for Masonry Walls Computations with Localisation of Damage – Part II. Computational Aspects, Submitted for Publication.

Page, A.W. (1981). The Biaxial Compressive Strength of Brick Masonry, *Proc. Instn Civ. Engrs., Part 2,* **71**: 893–906.

Page, A.W. (1983). The Strength of Brick Masonry under Biaxial Tension-compression, *International Journal of Masonry Constructions*, **3**: 26–31.

Papa, E. and Nappi, A. (1997). Numerical Modeling of Masonry: A Material Model Accounting for Damage Effects and Plastic Strains, *Applied Mathematics Modelling*, **21**: 319–335.

Peerlings, R.H.J., de Borst, R., Brekelmans, W.A.M. and de Vree, J.H.P. (1996). Gradient-enhanced Damage for Quasi-brittle Materials, *International Journal for Numerical Methods in Engineering*, **39**: 3391–3403.

Peerlings, R.H.J., Geers, M.G.D., de Borst, R., Brekelmans, W.A.M. (2001). A Critical Comparison of Nonlocal and Gradient-enhanced Softening Continua, *International Journal of Solids and Structures*, **38**: 7723–7746.

Peerlings, R.H.J., Massart, T.J. and Geers, M.G.D. (2004). A Thermodynamically Motivated Implicit Gradient Damage Framework and its Application to Brick Masonry Cracking, *Computer Methods in Applied Mechanics and Engineering*, **193**: 3403–3417.

Pijaudier-Cabot, R., Bažant, Z.P. (1987). Nonlocal Damage Theory, *Journal of Engineering Mechanics*, **113**: 1512–1533.

Raijmakers, T.M.J. and Vermeltfoort, A.T. (1992). Deformation Controlled Tests in Masonry Shear Walls (in Dutch), Technical Report B-92-1156, TNO – Bouw, Delft, The Netherlands.

Rice, J.R. (1976). The Localisation of Plastic Deformations, In: Koiter, W.T. (ed.), *Theoretical and Applied Mechanics*, North-Holland Publishing Company.

Rice, J.R. and Rudnicki, J.W. (1980). A Note on Some Features of the Theory of Localisation of Deformation, *International Journal of Solids and Structures*, **16**: 597–605.

Rots, J.G. (1997). Structural Masonry – An Experimental-numerical Basis for Practical Design Rules, A.A. Balkema, Rotterdam.

Sluys, L.J. and Berends, A.H. (1998). Discontinuous Failure Analysis for Mode-I and Mode-II Localisation Problems, *International Journal of Solids and Structures*, **35**(31–32): 4257–4274.

van der Pluijm, R. (1999). Out-of-plane Bending of Masonry – Behavior and Strength, PhD Thesis, Eindhoven University of Technology.

Wells, G.N. (2001). Discontinuous Modelling of Strain Localisation and Failure, PhD Thesis, Delft University of Technology.